

Multidecadal to multicentury scale collapses of Northern Hemisphere monsoons over the past millennium

Yemane Asmerom^{a,1}, Victor J. Polyak^a, Jessica B. T. Rasmussen^b, Stephen J. Burns^c, and Matthew Lachniet^d

^aDepartment of Earth and Planetary Sciences, University of New Mexico, Albuquerque, NM 87131; ^bLeander Independent School District, Leander, TX 78646; ^cDepartment of Geosciences, University of Massachusetts, Amherst, MA 01003; and ^dDepartment of Geoscience, University of Nevada, Las Vegas, NV 89154

Edited by Zhiming Kuang, Harvard University, Cambridge, MA, and accepted by the Editorial Board April 25, 2013 (received for review August 29, 2012)

Late Holocene climate in western North America was punctuated by periods of extended aridity called megadroughts. These droughts have been linked to cool eastern tropical Pacific sea surface temperatures (SSTs). Here, we show both short-term and long-term climate variability over the last 1,500 y from annual band thickness and stable isotope speleothem data. Several megadroughts are evident, including a multicentury one, AD 1350–1650, herein referred to as Super Drought, which corresponds to the coldest period of the Little Ice Age. Synchronicity between southwestern North American, Chinese, and West African monsoon precipitation suggests the megadroughts were hemispheric in scale. Northern Hemisphere monsoon strength over the last millennium is positively correlated with Northern Hemisphere temperature and North Atlantic SST. The megadroughts are associated with cooler than average SST and Northern Hemisphere temperatures. Furthermore, the megadroughts, including the Super Drought, coincide with solar insolation minima, suggesting that solar forcing of sea surface and atmospheric temperatures may generate variations in the strength of Northern Hemisphere monsoons. Our findings seem to suggest stronger (wetter) Northern Hemisphere monsoons with increased warming.

climate change | global warming | uranium series

Knowledge of regional expressions to past climate forcings and their associated atmospheric teleconnections is likely to be the key to building a unified global understanding of future climate change. The past one and one-half millennia, including the Medieval Climate Anomaly and Little Ice Age, is of particular interest because this period contains observed climate variability before a significant anthropogenic forcing, and thus represents important validation points for models of future climate change. One key climate phenomenon is the summer North American Monsoon System, which has been linked to changes in North Atlantic sea surface temperature (SST) indexed by the Atlantic Multidecadal Oscillation (AMO), whereby the positive phases of the AMO (warm North Atlantic SSTs) are associated with droughts (1). There is a strong linkage between the AMO and Northern Hemisphere temperature (NHT), such that the positive phase of the AMO coincides with warm NHT and vice versa (2). In addition, it was shown that southwestern North America winter precipitation is impacted by the Pacific Decadal Oscillation (PDO), whereby the positive phase of the PDO is associated with wetter than normal winters (3). Going back, the dominant view to date for southwestern North America is that the Medieval Climate Anomaly (*ca.* AD 900 to AD 1300) was a period of aridity and the Little Ice Age (*ca.* 1300 to the late 19th century) was less arid, although multiple decade-long droughts were also known to have occurred during the Little Ice Age (4, 5). This view of warmer being drier and cooler being wetter in southwestern North America is consistent with observations based on last glacial (6, 7) and Holocene climate (8) and was shown to reflect changes in the contribution of winter precipitation reflecting the position of the polar jet stream (8).

Here, we show, based on annually banded speleothem and supporting data, a contrasting picture of climate in which extended drought episodes are associated with cool NHT and that multidecadal droughts, including a multicentury drought that occurred at the beginning of the Little Ice Age, herein referred to as the Super Drought, are associated with the cold interval in Northern Hemisphere land and SSTs over the past 1,400 y. Conversely, pluvial periods are associated with warm NHT over this interval.

Stalagmite BC-11 was collected in 2004 from Bat Cave, a room in Carlsbad Cavern, New Mexico, while actively growing. It has apparent continuous annual banding; all of the uranium series dates, except two, fall within the band-counted age model within error (*SI Appendix, Fig. S1*, and *SI Appendix, Table S1*). $\delta^{13}\text{C}$ and $\delta^{18}\text{O}$ values were measured at an average interval of 10 y (Fig. 1*A* and *B*, respectively). In moisture-limited regions, such as southwestern North America, the thickness of annual growth bands is positively correlated to moisture amount (9, 10). Similarly, the stable isotopic data are interpreted to be relative wetness indicators. Because Bat Cave relative humidity today varies between 70% and 95%, dry conditions are interpreted, in part, to reflect greater kinetic fractionation, resulting in higher $\delta^{13}\text{C}$ and $\delta^{18}\text{O}$ values in the stalagmite calcite. Another influence on stalagmite $\delta^{18}\text{O}$ values are variations in moisture sources, with lower δD and $\delta^{18}\text{O}$ values derived from Pacific-dominated moisture and higher values from Gulf of Mexico and Gulf of California-dominated moisture (6, 11, 12). Variations in stalagmite $\delta^{18}\text{O}$ values could thus also contain imprints related to changes in air temperature, seasonality, amount of rainfall, and other factors (13). However, large temperature changes are unlikely to be enough to cause significant stalagmite $\delta^{18}\text{O}$ variations (Fig. 1*B*) relative to the much larger variations associated with moisture source.

In contrast to $\delta^{18}\text{O}$, $\delta^{13}\text{C}$ variability in stalagmite calcite reflects local conditions. Drier than normal periods likely result in lower soil productivity, slower infiltration rates with greater bedrock carbon proportion (higher $\delta^{13}\text{C}$ values relative to soil-derived carbon), and possibly enhanced kinetic fractionation, all of which could result in high speleothem calcite $\delta^{13}\text{C}$ values (13). Conversely, greater regional precipitation equates to more vegetation, more productive soils, and more soil CO_2 production, all producing more negative $\delta^{13}\text{C}$ values. Support for this interpretation is the negative correlation ($r = -65$, $P < 0.001$; see *SI Appendix* for complete discussion of statistical treatment) between speleothem band thickness and $\delta^{13}\text{C}$ (Fig. 1*A*). Similarly, there is a slightly

Author contributions: Y.A. designed research; Y.A., V.J.P., J.B.T.R., and S.J.B. performed research; Y.A., V.J.P., J.B.T.R., and S.J.B. contributed new reagents/analytic tools; Y.A., V.J.P., J.B.T.R., S.J.B., and M.L. analyzed data; and Y.A. wrote the paper.

The authors declare no conflict of interest.

This article is a PNAS Direct Submission. Z.K. is a guest editor invited by the Editorial Board.

¹To whom correspondence should be addressed. E-mail: asmerom@unm.edu.

This article contains supporting information online at www.pnas.org/lookup/suppl/doi:10.1073/pnas.1214870110/-DCSupplemental.

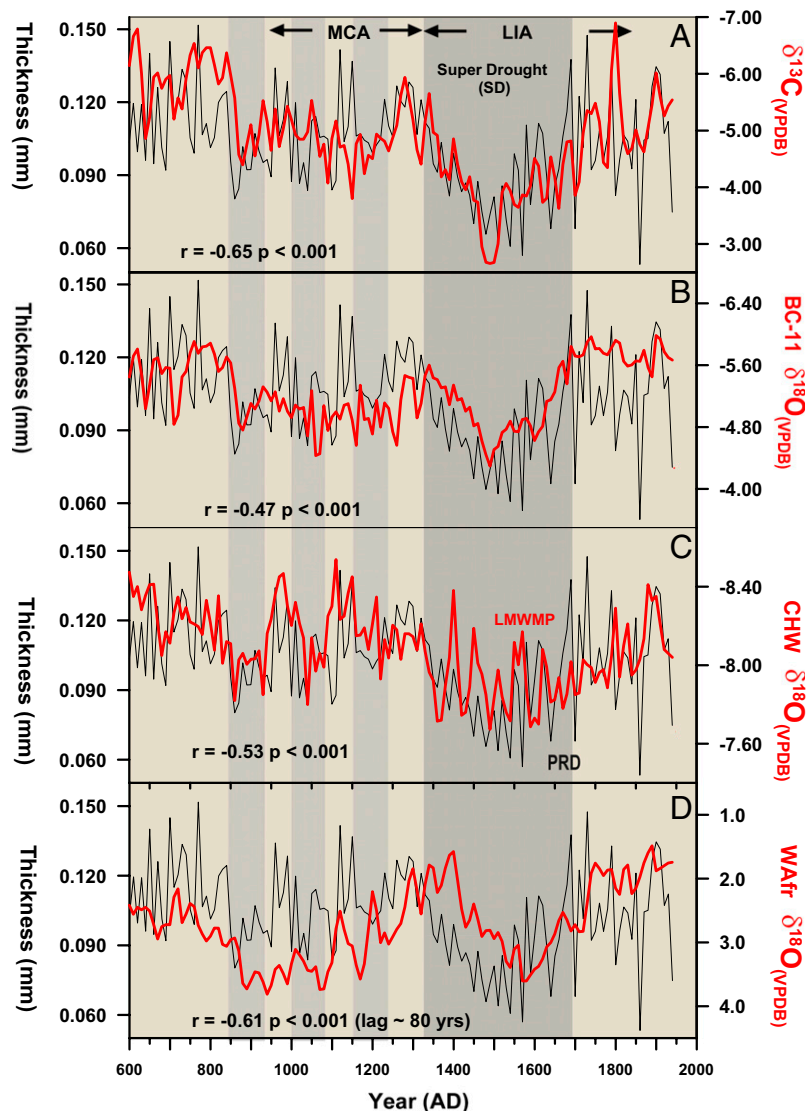


Fig. 1. Comparison between stalagmite BC-11 thickness of annual growth bands BC-11 $\delta^{13}\text{C}$, and $\delta^{18}\text{O}$ isotopic data, stalagmite $\delta^{18}\text{O}$ isotopic data from Wanxiang Cave, China (16), and lake sediment $\delta^{18}\text{O}$ isotopic data from West Africa (20) tree ring chronology from a site located near the BC-11 site (Guadalupe Peak) (15). The annual band thickness data were smoothed and sampled at 10-y interval evenly (the average resolution of the isotopic data) for statistical analysis. (A) The BC-11 speleothem band thickness and BC-11 $\delta^{13}\text{C}$ show significant correlation ($r = -0.65$, $P < 0.001$). The Super Drought and other megadroughts (gray vertical bars) are shown as a prolonged period of high $\delta^{13}\text{C}$ and low band thickness; the Super Drought contains the lengthiest and most severe drought period for the entire record. (B) The BC-11 growth data are compared with $\delta^{18}\text{O}$ isotopic data. The growth data and $\delta^{18}\text{O}$ data show significant correlation ($r = -0.47$, $P < 0.001$) but less than the growth – $\delta^{13}\text{C}$ data. (C) The BC-11 growth data plotted against speleothem $\delta^{18}\text{O}$ East Asian monsoon precipitation proxy data from China (Wanxiang Cave) (CHW) (16) because it was previously shown that there is a seesaw response between the two regimes during Holocene (8) and Glacial (6) climate variability. In contrast, during the Medieval Climate Anomaly–Little Ice Age period, both regions were experiencing similar pluvial and drought episodes. There is significant correlation between the two records ($r = -0.53$, $P < 0.001$), but more importantly, the megadroughts match well. There is a mismatch between the peak of the Pueblo Revolt Drought (PRD) and the Late Ming Weak Monsoon Period (LMWMP). The PRD monsoon drought in our record is obscured growth from winter moisture. (D) There is broad agreement between the lake sediment $\delta^{18}\text{O}$ data from the West African and BC-11 stalagmite growth data. The best match ($r = -0.61$, $P < 0.001$) is achieved if the records are shifted by about 80 y, which is allowable within the age constraints of the varve sediments (18).

weaker but significant ($r = -0.47$, $P < 0.001$) negative correlation between $\delta^{18}\text{O}$ and growth thickness, supporting our interpretation of an effective moisture forcing on stalagmite $\delta^{18}\text{O}$ values. Both of these correlations are consistent with previous observations that support a link between speleothem band thickness and precipitation in this region (10). The lower smaller correlation between $\delta^{18}\text{O}$ and growth thickness may be in part due to moisture source $\delta^{18}\text{O}$ variability, which seasonally varies between $-6.2 \pm 2.7\text{‰}$ for summer moisture to $-11.3 \pm 3.5\text{‰}$ for winter Pacific-sourced moisture (8, 14), both of which are less tied to local climatic conditions than the $\delta^{13}\text{C}$.

In Fig. 1C, we show the BC-11 data plotted against speleothem $\delta^{18}\text{O}$ East Asian monsoon precipitation proxy data from Wanxiang Cave, China (13). There is significant correlation between BC-11 growth banding and the Chinese $\delta^{18}\text{O}$ data ($r = -0.53$, $P < 0.001$), and BC-11 $\delta^{13}\text{C}$ and the Chinese $\delta^{18}\text{O}$ data ($r = 0.50$, $P < 0.05$). The major features and, in particular, the most severe drought interval during the early Little Ice Age are also replicated in other speleothems from the same cave and other caves in the region (*SI Appendix, Fig. S2 B and C*, and *SI Appendix, SI Text*). The growth banding and local Guadalupe tree ring chronology (15) match reasonably well (Fig. 1C; $r = 0.42$, $P < 0.01$).

The discrepancy between speleothem band thickness and the local tree ring chronology (Fig. 1C) around 1650 may be related to seasonality sensitivity difference between speleothem (interpreted to be a summer monsoon proxy) and tree rings (growing season sensitive). This is discussed further when comparing our speleothem data to a winter precipitation-dominated area (Fig. 2B).

The speleothem band thickness and $\delta^{13}\text{C}$ and $\delta^{18}\text{O}$ isotopic data (Fig. 1A and B) show the Medieval Climate Anomaly–Little Ice Age interval to have been a time of extreme climate variability, punctuated by multidecadal dry periods (here referred to as megadroughts), some of which were previously shown to have been spatially extensive throughout the western United States (4). Here, we identify a particularly extended multicentury dry period, the Super Drought, occurring during the early Little Ice Age ca. AD 1350–1650. Our multiple speleothem records show this period of drought in southwestern North America as the most severe over the last 2,000 y (*SI Appendix, Fig. S2A and B*) (10). The Medieval Climate Anomaly overall, by our interpretation, was punctuated by multiple megadroughts that interrupted multiple pluvials, and does not represent the driest period of the past 1,400 y.

Remarkably, the inverse relationship between southwestern North America and East Asian monsoon region precipitation amount previously documented for the Holocene (8), and for the Last Glacial period (6), is reversed during the Medieval

Climate Anomaly and Little Ice Age (Fig. 1C). In contrast, there is a positive correlation between contemporaneous strong monsoon events in both regions (Fig. 1C) over this period. Moreover, the megadroughts recorded in BC-11 match the droughts reported in the China stalagmite (16), which is linked to the decline of Chinese dynasties (Fig. 1C) (16) within an estimated error of about ± 15 y for the Chinese record (16) and a maximum error of ± 10 y for our growth banding (see *SI Appendix* for discussion on statistical treatment and plotting of data). The only notable exception is the mismatch between the Late Ming Weak Monsoon Period drought in China and the Pueblo Revolt Drought in southwestern North America (Fig. 1C). There are supporting historical records from the later part of the Super Drought. The most severe interval of the 1600s drought in the southwestern North America, as constrained by historical documentation (17, 18), was during the 1660s and 1670s and was summer drought in conjunction with long and snowy winters. The timing of the most prominent drought, the Super Drought, is also a time of extended drought in the East Asian monsoon region (16) (Fig. 1C).

Other regional ocean–atmosphere teleconnections show similar timing of severe droughts during the Medieval Climate Anomaly–Little Ice Age interval. Today, warm North Atlantic SST anomalies (positive AMO) are associated with a stronger West African monsoon (19, 20), whereas the reverse is the case for southwestern

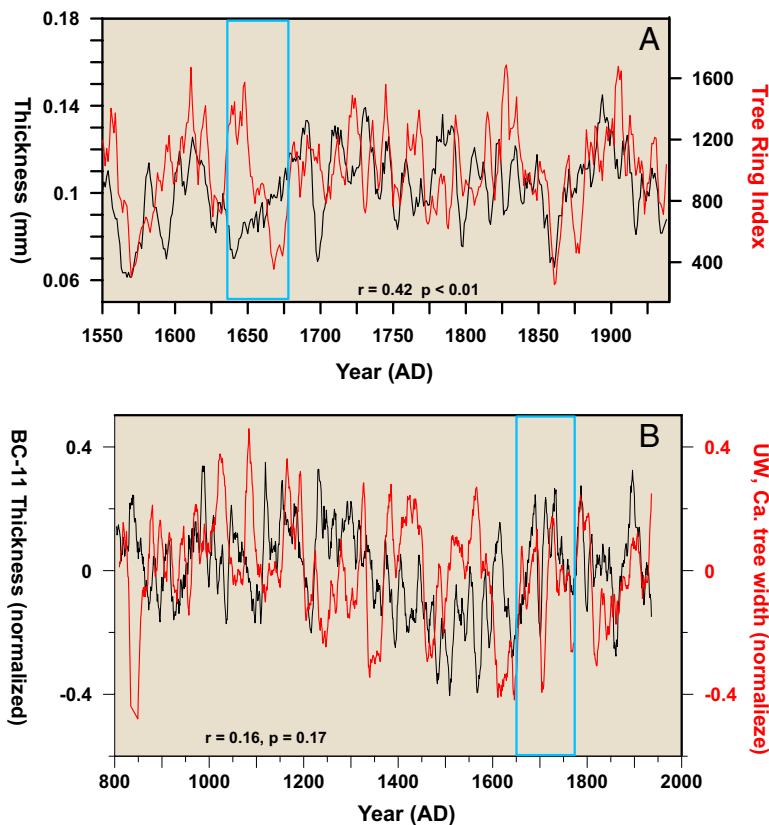


Fig. 2. BC-11 stalagmite growth compared with local tree ring chronology (sensitive to growing season, North American summer monsoon) and tree ring chronology from the Sierra Nevada, which gets its moisture during the winter. (A) The speleothem growth and the tree ring chronology from the Guadalupe Peak (a site near the BC-11 site) shows that the two records track each other reasonably well at greater than decadal timescales. There is a marked divergence around ca. AD 1650 (blue box), which is likely attributable to sensitivity difference between tree rings (growing season) and speleothems, which reflect annual effective moisture. Based on historical documents, the 1660s drought, the Pueblo Rebellion Drought was a summer (monsoon) drought with unusually long, cold, and snowy winters (17, 18). The same time shown in Fig. 2B (below) is coherent with the tree ring chronology that reflects winter precipitation. (B) Comparison between BC-11 growth-banding data and tree ring chronology from Sierra Nevada, California (Upper Wright Lakes) (21), representing the southern portion of the north–south dipole of winter precipitation response to PDO variability (3, 9). The lack of coherence between the two records suggest that precipitation variability in southwestern North America during the coverage time is likely dominated by summer North American monsoon precipitation. Note: the interval in which the BC-11 diverges from the local tree ring data (Fig. 2A, blue box) is coherent with the winter-sensitive chronology here (blue box).

North America (1). This dipole response by the two monsoon regions to AMO forcing likely reflects the relative strength and position of the Bermuda (Azores) High (1). Here, in contrast to the short-term (AMO-driven) precipitation dipole, the two monsoon regions seem to be responding coherently during the extended drought and pluvial episodes (Fig. 1*D*; $r = -0.611$, $P < 0.001$). There is a lag of 80 y (our speleothem data leading) for a maximum match between the two records, which is clearly discernible in Fig. 1*D* but may be mostly due to uncertainties in the varve chronology (20). The coincidence of the drought intervals, and in particular the Super Drought, in all of these records, suggests that these multi-decadal to multicentury scale droughts are hemispheric in scale.

Southwestern North America receives both winter (dominantly Pacific) and summer (dominantly North American monsoon) precipitation. The winter precipitation is part of a northwestern North America and southwestern North American precipitation dipole (3, 9). Therefore, we compared our record with a record from part of the southern dipole that mostly gets its moisture from winter precipitation, to establish whether the megadroughts are due to summer monsoon deficit or winter Pacific-sourced moisture deficit. The Upper Wright Lakes tree ring chronology (21), from the Sierra Nevada Mountains, California, is the furthest southern record with continuous appreciable time coverage that represents winter (Pacific-dominated) moisture. The tree ring chronology is plotted with the BC-11 growth thickness data (Fig. 24). The two records are normalized to their means [(sample - mean)/mean], and thus the values are dimensionless. The Upper Wright Lakes location is further north than would be desirable (N36.62°, W118.37°). Nevertheless, the graph shows that the two records are not coherent with a nonsignificant low correlation ($r = 0.16$, $P = 0.17$). Consequently, their pluvials and droughts are not synchronous, suggesting that the southwestern North America droughts reflect summer rather than winter moisture deficits. Of particular note is the only interval where there is coherence between these two records, during the latter half of the Little Ice Age (Fig. 24, blue box). It shows that the late Little Ice Age pluvial event in our study area is likely winter dominated. Based on historical data, the height of the Pueblo Revolt Drought was 1660–1670 and was characterized by severe summer droughts and long, cold, and snowy winters (17, 18). It is thus not surprising the discrepancy between our speleothem growth-based precipitation proxy (which is less sensitive to seasonality) and the Guadalupe Mountains tree ring-based proxy (Fig. 24, blue box), which is likely to be dominated by growing season (summer) growth.

In Fig. 3*A* and *B*, we show our speleothem band thickness and $\delta^{13}\text{C}$ data plotted against NHT anomaly data (22) starting at 700 AD (a common interval for the proxies shown in Fig. 3). During this interval, there is a strong and significant correlation between the growth banding data and the $\delta^{13}\text{C}$ isotope data ($r = -0.81$, $P < 0.001$) and the NHT anomaly data, with the best match achieved with a lag of 60 y (NHT leading) ($r = 0.82$, $P < 0.001$). The lag is very sensitive to the size of lag window used and therefore we do not assign a mechanistic significance at this point (see *SI Appendix* for discussion on statistical treatment). Although there is a strong and significant correlation between our precipitation proxy data and NHT data, we cannot be certain that there is a causal relationship between the two and they may be responding to a different but common forcing. In Fig. 3*C*, we show the band growth data plotted against SST from Chesapeake Bay, North Atlantic (23). This record is not necessarily a space-averaged representation of North Atlantic SST, but the good correlation ($r = 0.43$, $P < 0.001$) suggests that North Atlantic SST variability may have significant role in Northern Hemisphere megadrought and pluvial variability.

Potential external forcing of North Atlantic SST variability also has to be considered. We previously showed that during most of the Holocene (8) high solar activity is associated with dry conditions in southwestern North America and pluvial conditions in

East Asian monsoon regions (8). In Fig. 3*D*, we compare our results to a solar variability proxy [as total solar irradiance (TSI)], which is based on the production of cosmogenic Be (24, 25) and is dominantly modulated by variability in solar activity. Data based on radiocarbon (^{14}C) production (26) show similar patterns. Our growth-banding data and the TSI data show a surprising positive correlation ($r = 0.56$, $P < 0.001$) between our band thickness record and the TSI with a lag of approximately -40 y (TSI leading). The core of the Super Drought coincides with the Spörer Minimum. There is not a distinct drought associated with the Wolf Minimum, but it does occur during the initiation of the Super Drought. The Maunder Minimum roughly coincides with a severe drought with historical documentation, the previously discussed Pueblo Revolt Drought. The Spanish occupation of southwestern North America took place in the midst of one of the most severe droughts of the last two millennia.

We do not have a full mechanistic understanding of solar modulation of monsoon strength over the timescales involved. Cooler SSTs and cooler NHT by themselves should lower specific humidity of the Northern Hemisphere atmosphere. However, solar modulation is likely to involve complicated ocean-atmosphere interactions. For example, general circulation model simulations of the short 11-y solar cycle show bidirectional ocean-atmosphere coupled interaction with strong impact on North Atlantic Oscillation (NAO) (27), which has been shown to impact the Asian monsoon for example (28). The coherent occurrence of megadroughts in Northern Hemisphere monsoons is different in comparison with short-term climate variability associated with the NAO or its corresponding SST expression, the AMO. NAO or AMO variability results in contrasting response by the different Northern Hemisphere monsoons. For example, the North America monsoon response to AMO variability is opposite of that of the West African monsoon (1, 19). As a result, the NAO or AMO variability may not be appropriate analogs for climate variability during the megadroughts. Hemisphere-scale changes, such as changes in the specific humidity, or strength and extent of the Hadley cell in response to solar modulation, as suggested by some workers (29), may be more applicable. We have not formally looked at Southern Hemisphere monsoons. Recent analysis (30) shows that the South American monsoon was at its strongest during the period of the Northern Hemisphere Super Drought, hinting at a global monsoon precipitation dipole during the Medieval Climate Anomaly-Little Ice Age time interval.

Our analysis suggests that Northern Hemisphere monsoon megadroughts over the past 1.5 millennia are associated with cold Northern Hemisphere and SSTs and intervals of low solar irradiance, whereas pluvials are associated with the opposite patterns. These data suggest that monsoon strength may be attributed to variations in specific humidity associated with varying SST. If this relationship remains valid under the altered atmospheric circulation patterns of an anthropogenically altered climate, then future monsoon responses may become stronger. This inference seems to be supported by recent instrumentally based observations (31) and model results (32, 33).

Materials and Methods

U-series isotope measurements were made at the Radiogenic Isotope Laboratory, University of New Mexico. Subsample powders (50–200 mg) were drilled and dissolved in nitric acid and spiked with a mixed ^{229}Th - ^{233}U - ^{236}U spike. U and Th were separated using conventional anion-exchange chromatography. Most of the U and Th measurements were made on a Micro-mass Sector 54 thermal ionization mass spectrometer (TIMS). Those subsamples designated with an “M” at the end of the sample name were measured with a Neptune multicollector inductively coupled plasma mass spectrometer (MC-ICPMS). The TIMS measurements were done using an ion-counting Daly multiplier by peak-jumping U and Th isotopes (10). The MC-ICPMS measurements were run in static mode using a mix of 10^{11} and 10^{12} Ω resistors in conjunction with five Faraday cup detectors and an ion-counting secondary electron multiplier detector, following

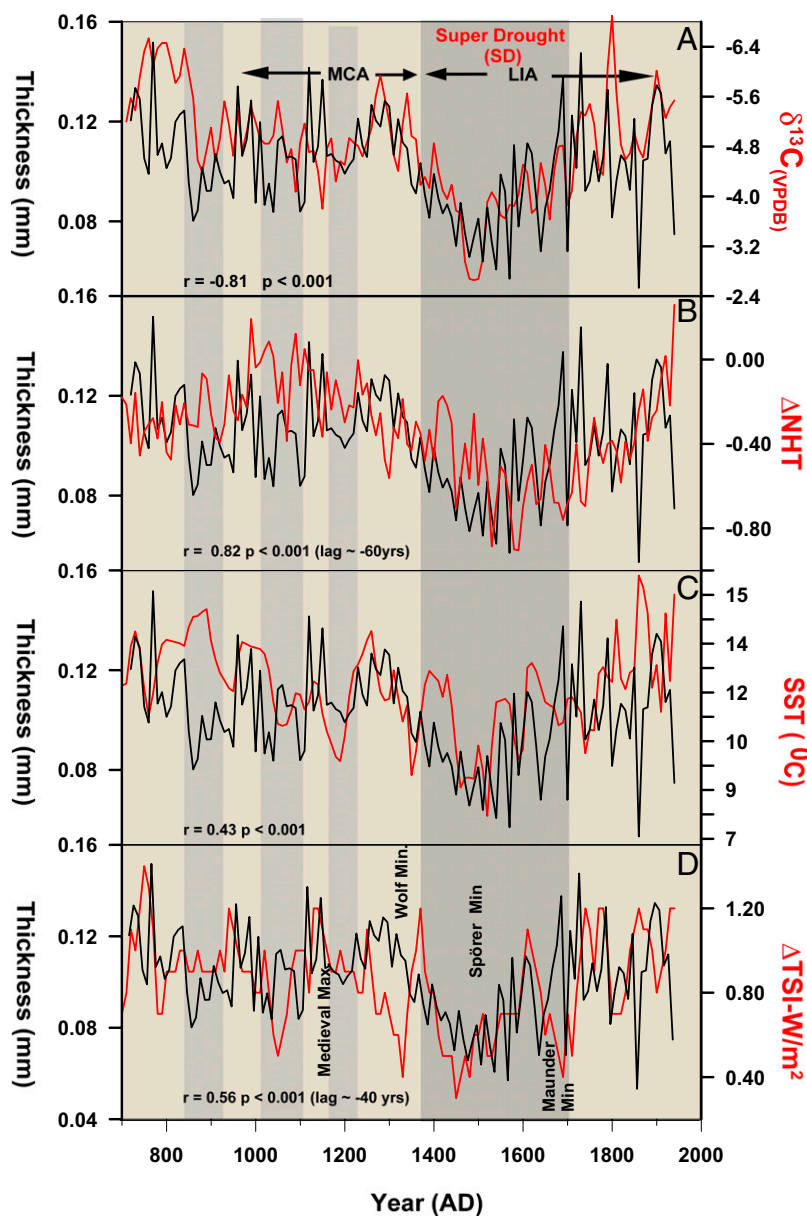


Fig. 3. BC-11 speleothem growth band thickness and $\delta^{13}\text{C}$ data plotted against NHT reconstruction (22), SST data from Chesapeake Bay (23), and cosmogenic isotopes (^{10}Be)-based total solar irradiance (TSI) data (24, 25) over the past 1,300 y (a time interval common to all of the records). (A) The match between the band thickness and $\delta^{13}\text{C}$ data over this interval is remarkable ($r = -0.81$, $P < 0.001$), consistent with the inference that the band thickness and $\delta^{13}\text{C}$ are tracking a common climatic variable. (B) There is a positive correlation between NHT (22) data and southwestern North America precipitation (speleothem band thickness data); the best match is achieved with a lag (NHT leading) of 60 y ($r = 0.82$, $P < 0.001$). The megadroughts occur during NHT lows; the Super Drought happened during the lowest extended cold period in the Northern Hemisphere. (C) North Atlantic sea surface (SST) data from the Chesapeake Bay (23) plotted against BC-growth thickness data. The two datasets match broadly ($r = 0.42$, $P < 0.001$). (D) Cosmogenic isotopes (^{10}Be)-derived estimates of total solar irradiance (TSI) plotted against our band growth data. The two are positively correlated ($r = 0.56$, $P < 0.001$), which is the opposite of the long-term (Holocene) relationship we previously described (8). The distinct discordance between the two records is the fact that the Maunder Minimum seems associated with a pluvial period.

the method described in ref. 34. The CRM-145 U isotope standard was measured with the samples, obtaining the conventionally accepted $\delta^{234}\text{U}$ value of -36.5 (34). U and Th procedural blanks were in the range of 5–10 pg and therefore have no effect on ages. The analytical uncertainties are 2σ of the mean. The age uncertainties include analytical errors and uncertainties in the initial $^{230}\text{Th}/^{232}\text{Th}$ ratios. Initial $^{230}\text{Th}/^{232}\text{Th}$ ratios were corrected using an empirical relationship between Th concentration and initial $^{230}\text{Th}/^{232}\text{Th}$ ratios, as follows: $X = 0.0033 \times [^{232}\text{Th ppt}]^{-0.6664} \pm 100\%$, where $X = \text{initial } ^{230}\text{Th}/^{232}\text{Th} \text{ atomic ratio}$.

The $\delta^{18}\text{O}$ and $\delta^{13}\text{C}$ values were measured at the University of Massachusetts Stable Isotope Laboratory. Subsamples were drilled with a 0.5-mm-diameter bit along the stalagmite BC-11 growth axis at a 10-y sampling

interval. Stalagmite powders were reacted with a few drops of anhydrous phosphoric acid at 70 °C in a Finnigan Kiel-III automated carbonate preparation device directly coupled to a Finnigan Delta Plus ratio mass spectrometer. Results are reported in standard permil (‰) notation with respect to Vienna Pee Dee Belemnite (VPDB). Internal precision is $\sim 0.1\%$ for $\delta^{18}\text{O}$ and $\delta^{13}\text{C}$.

ACKNOWLEDGMENTS. We thank D. Pate, S. Allison, Carlsbad Caverns National Park, the late R. Turner, and Lincoln National Forest, for collection permits and field assistance. P. Provencio and S. Bono also provided field assistance. This work was supported by National Science Foundation Grants ATM-0214333 (to V.J.P. and Y.A.), ATM-0703353 (to Y.A. and V.J.P.), and EAR-0326902 (to Y.A. and others).

1. McCabe GJ, Palecki MA, Betancourt JL (2004) Pacific and Atlantic Ocean influences on multidecadal drought frequency in the United States. *Proc Natl Acad Sci USA* 101(12): 4136–4141.
2. Wyatt MG, Kravtsov S, Tsonis AA (2011) Atlantic Multidecadal Oscillation and Northern Hemisphere's climate variability. *Clim Dyn*, 10.1007/s00382-011-1071-8.
3. MacDonald GM, Case RA (2005) Variations in the Pacific Decadal Oscillation over the past millennium. *Geophys Res Lett* 32:L08703, 10.1029/2005GL022478.
4. Cook ER, Woodhouse CA, Eakin CM, Meko DM, Stahle DW (2004) Long-term aridity changes in the western United States. *Science* 306(5698):1015–1018.
5. Swetnam TW, et al. (2009) Multi-millennia fire history of the Giant Forest, Sequoia National Park, USA. *Fire Ecol* 5:117–147.
6. Asmerom Y, Polyak V, Burns S (2010) Variable winter moisture in the southwestern United States linked to rapid glacial climate shifts. *Nat Geosci* 3:114–117.
7. Wagner JDM, et al. (2010) Moisture variability in the southwestern United States linked to abrupt glacial climate change. *Nat Geosci* 3:110–113.
8. Asmerom Y, Polyak V, Burns S, Rasmussen J (2007) Solar forcing of Holocene climate: New insights from a speleothem record, southwestern USA. *Geology* 35:1–4.
9. Rasmussen JBT, Polyak VJ, Asmerom Y (2006) Evidence for Pacific modulated precipitation variability during the late Holocene from the southwestern USA. *Geophys Res Lett* 33:L08701, 10.1029/2006GL025714.
10. Polyak VJ, Asmerom Y (2001) Late Holocene climate and cultural changes in the southwestern United States. *Science* 294(5540):148–151.
11. Yapp CJ (1985) D/H variations of meteoric waters in Albuquerque, New Mexico, USA. *J Hydrol (Amst)* 76:63–84.
12. Strong M, Sharp ZD, Gutzler DS (2007) Diagnosing moisture transport using D/H ratios of water vapor. *Geophys Res Lett*, 10.1029/2006GL028307.
13. Lachniet MS (2009) Climatic and environmental controls on speleothem oxygen isotope values. *Quat Sci Rev* 28:412–432.
14. Sharp Z (2007) *Principles of Stable Isotope Geochemistry* (Pearson/Prentice Hall, Upper Saddle River, NJ), 1st Ed, p 344.
15. Stahle DW, Montagu N, Cleaveland MK (1992) *IGBP Pages/World Data Center for Paleoclimatology Data Contribution Series tx-046* (NOAA/NGDC Paleoclimate Program, Boulder, CO).
16. Zhang P, et al. (2008) A test of climate, sun, and culture relationships from an 1810-year Chinese cave record. *Science* 322(5903):940–942.
17. Schroeder AH (1972) *Rio Grande Ethnohistory. New Perspectives on the Pueblos*, ed Ortiz A (Univ of New Mexico Press, Albuquerque, NM), pp 41–70.
18. Silberg R (1970) *The Pueblo Revolt* (Univ of Nebraska Press, Lincoln, NE).
19. Elsa Mohino E, Janicot S, Bader J (2009) Sahel rainfall and decadal to multi-decadal sea surface temperature variability. *Clim Dyn*, 10.1007/s00382-010-0867-2.
20. Shanahan TM, et al. (2009) Atlantic forcing of persistent drought in West Africa. *Science* 324(5925):377–380.
21. Lloyd AH, Graumlich LJ (1997) Holocene dynamics of treeline forests in the Sierra Nevada. *Ecology* 78:1199–1210.
22. Moberg A, et al. (2005) Highly variable Northern Hemisphere temperatures reconstructed from low- and high-resolution proxy data. *Nature* 433(7026):613–617.
23. Cronin TM, Dwyer GS, Kamiya T, Schwede S, Willard DA (2003) Medieval Warm Period, Little Ice Age and 20th century temperature variability from Chesapeake Bay. *Global Planet Change* 36:17–29.
24. McCracken KG, et al. (2004) A phenomenological study of the longterm cosmic ray modulation, 850–1958 AD. *J Geophys Res*, 10.1029/2004JA010685.
25. Webber WR, Higbie PR (2003) Production of cosmogenic Be nuclei in the Earth's atmosphere by cosmic rays: Its dependence on solar modulation and the interstellar cosmic ray spectrum. *J Geophys Res*, 10.1029/2003JA009863.
26. Stuiver M, et al. (1998) INTCAL98 radiocarbon age calibration, 24000-0 cal BP. *Radiocarbon* 40:1041–1083.
27. Scaife AA, et al. (2013) A mechanism for lagged North Atlantic climate response to solar variability. *Geophys Res Lett*, 10.1002/grl.50099.
28. Linderholm HW, et al. (2011) Interannual teleconnections between the summer North Atlantic Oscillation and the East Asian summer monsoon. *Geophys Res Lett*, 10.1029/2010JD015235.
29. Gray LJ, et al. (2010) Solar influences on climate. *Rev Geophys* 48:RG4001, 10.1029/2009RG000282.
30. Vuille M, et al. (2012) A review of the South American monsoon history as recorded in stable isotopic proxies over the past two millennia. *Climate of the Past* 8:1309–1321.
31. Wang B, et al. (2013) Northern Hemisphere summer monsoon intensified by mega-El Niño/southern oscillation and Atlantic multidecadal oscillation. *Proc Natl Acad Sci USA* 110(14):5347–5352.
32. Pang-chi H, et al. (2012) Increase of global monsoon area and precipitation under global warming: A robust signal? *Geophys Res Lett* 39:L06701 703, 10.1029/2012GL051037.
33. Held IM, Soden BJ (2006) Robust responses of the hydrological cycle to global warming. *J Clim* 19:5686–5699.
34. Asmerom Y, Polyak V, Schwieters J, Bouman C (2006) Routine high-precision U-Th isotope analyses for paleoclimate chronology. *Geochim Cosmochim Acta* 70:18–24.